JOURNAL OF PROPULSION AND POWER
Vol. 16, No. 6, November–December 2000

Application of Bethe–Zel'dovich–Thompson Fluids in Organic Rankine Cycle Engines

Brady P. Brown*
Krispin Technologies, Inc., Rockville, Maryland 20850
and
Brian M. Argrow†
University of Colorado, Boulder, Colorado 80309-0429

The novel concept of improving organic Rankine cycle engines (ORCEs) by exploiting the unusual fluid dynamic behavior of a special class of working fluids known as Bethe–Zel'dovich–Thompson (BZT) fluids is explored. ORCEs are currently manufactured and used for numerous remote terrestrial applications requiring reliable, unattended power. One of the major loss mechanisms in ORCEs is shock waves generated in the turbine stage. Operating under the proper thermodynamic conditions, a BZT working fluid can potentially weaken or eliminate shock waves. This would reduce losses due to both the wave drag from shocks as well as losses from boundary-layer separation due to shock reflections on the turbine blades. Two-dimensional flowfields through realistic symmetric impulse turbine cascades are compared using a flux-limited, finite difference numerical scheme to assess differences in flow efficiencies. Results show significant improvements in turbine efficiencies for BZT working fluids over conventional ORCE working fluids.

Nomenclature

A	=	state equation constant
a	=	speed of sound
B	=	state equation constant
b	=	state equation constant
b'	=	force parameter
C	=	state equation constant
C_0	=	isentropic spouting velocity
c	=	chord
d	=	blade separation distance
E_H	=	hydraulic turbine efficiency
k	=	state equation constant
M	=	Mach number
p	=	pressure
R	=	gas constant
s	=	specific entropy
T	=	temperature
t	=	blade thickness
U	=	rotor tip speed
u	=	streamwise component of velocity
$\boldsymbol{V}$	=	velocity
v	=	transverse component of velocity
x	=	streamwise spatial coordinate
y	=	transverse spatial coordinate
α	=	covolume parameter
β	=	outflow angle relative to turbine cascade
Γ	=	fundamental derivative of gasdynamics
γ	=	ratio of specific heats
θ	=	absolute inflow angle
ρ	=	density
υ	=	specific volume
φ	=	inflow angle relative to turbine cascade
ψ	=	rotor velocity coefficient

Subscripts

c	=	critical point
1	=	inflow boundary
2	=	outflow boundary

Received 13 March 1999; revision received 12 November 1999; accepted for publication 28 December 1999.

*Research Scientist, 1370 Piccard Drive, Suite 210; brady@krispintech.com.

†Assistant Professor, Department of Aerospace Engineering Sciences; argrow@polaris.colorado.edu.

I. Introduction

As the inevitable exhaustion of fossil fuels looms ever closer, the exploration of alternative energy sources becomes increasingly important. One appealing option for low-power applications is the organic Rankine cycle engine (ORCE). Similar to the large steam Rankine cycle engines used in electric power plants, an ORCE utilizes heavy working fluids and has superior efficiency compared to steam Rankine cycle engines for heat source temperatures below around 900 K. An ORCE typically requires only a single-stage expander, making the ORCE much simpler than multistage steam systems. Such simplicity also gives the ORCE an obvious advantage over other types of small engines that are more mechanically complex, for example, typical two- or four-stroke engines as well as the Stirling engine.

For the past several decades, thousands of ORCEs have been developed and used for remote terrestrial applications with power outputs ranging from 1 to 1000 kW (Ref. 1). A few examples of remote applications that have used efficient, reliable, unattended ORCE power sources include communication stations, data gathering buoys, and satellite communication power supplies,[2] as well as irrigation pumps, air conditioners, and turbogenerators.

The most recent developments in ORCE technology have focused on using renewable energy resources. Several ORCEs powered by solar energy have been successfully built and demonstrated[3,4] including solar-dish engines.[5] Two advantages such a device has over photovoltaic generated electricity are higher efficiency and smaller space requirements. ORCEs used to produce power from geothermal sources have also been developed and successfully demonstrated.[5] In addition, three U.S. companies have developed ORCEs for use with waste heat streams resulting from industrial processes.[6,7]

ORCE working fluids are heavy organic compounds that possess large heat capacities, for example, toluene (C_7H_8) and R-113 ($C_2Cl_3F_3$). Interestingly, several of the organic fluids proposed and used in ORCEs have the potential to exhibit unusual fluid dynamic phenomena in the thermodynamic regime above the coexistence curve, near the liquid–vapor critical point. Such phenomena include

expansion shock waves, disintegrating shocks, splitting shocks, composite waves (e.g., shock-fan combinations), as well as reversal of wave type on reflection. Fluids that exhibit unique flow properties such as these are sometimes referred to as Bethe–Zel'dovich–Thompson (BZT) fluids in recognition of the three investigators who first postulated their existence.[8]

Previous ORCE development efforts have never attempted to take advantage of BZT gasdynamic behavior. One of the major losses in ORCEs occurs through the generation of shock waves in the turbine. The unique flow properties of BZT fluids may significantly reduce losses due to shock waves or even allow supersonic shock-free turbine expansion. Thus, ORCEs that utilize BZT working fluids, hereafter referred to as BZT–ORCEs, can potentially obtain higher efficiencies than ORCEs using conventional working fluids.

The recent interest and investigation in gasdynamics for heavy fluids near the critical point have birthed a relatively new area of science known as dense gasdynamics. To clarify, a dense gas refers to a fluid with thermodynamic conditions in the vicinity of the liquid–vapor critical point. The phrase dense gas regime refers to the aforementioned thermodynamic region, and dense gas flow indicates all or part of a flowfield with thermodynamic states in the dense gas regime. Discussed in detail in the next section, a BZT fluid is a dense gas that can exhibit unusual gasdynamic properties for flows completely in the vapor phase.

Many aspects of dense gas theory are well developed and understood. Much analytical investigation has been performed for both the inviscid and viscous structure of dense gas phenomena (see Refs. 8 and 9 as examples and sources for further references). Various numerical techniques have also been utilized to investigate dense gas phenomena. Cramer et al.[10] simulate evolving wave fields of weakly dissipative, small-amplitude disturbances with mixed nonlinearity. Thompson et al.[11] numerically model dense gas flow to complement multiphase shock-tube flow experiments where two-phase split shocks and two-phase expansion shocks are observed. Argrow[12] simulates the evolution of wave fields for one-dimensional flows of BZT gases. Solutions to nonclassical Reimann problems are observed to demonstrate expansion shocks, splitting shocks, composite waves, and reversal of wave type on reflection. Brown and Argrow[13] extend the investigation of BZT wave fields for two-dimensional flows. Transient BZT gas flowfields for moving shocks incident on compressive wedges and circular arcs are found to be strikingly different from the classical wave fields of dilute gases. Numerical simulations of steady BZT gas flowfields also show significant qualitative differences in structure from analytical formulations and experimental observations of dilute gases.[14]

The utilization of BZT fluids in technology has already been investigated to some extent. Aldo and Argrow,[15] Anders,[16] Kluwick,[17] Schnerr and Leidner,[18] and Anderson[19] have investigated the application of BZT fluids in nozzles and heavy-gas wind tunnels. Schnerr and Leidner[20] numerically demonstrate reduced losses in transonic axial cascade flows with simple blade geometries for BZT fluids. An isentropic supersonic flow through a cascadelike channel is shown by Monaco et al.[21] ORCEs commonly have supersonic inflow at the turbine with Mach numbers ranging from $1 < M_{in} < 2$ (Ref. 22). To the authors' knowledge, the work presented here is the first investigation for supersonic dense gas flow through realistic turbine cascades. In addition, the work presented here is the first direct comparison of turbine cascade flows for BZT fluids with conventional ORCE working fluids through quantitative performance parameters such as pressure loss and turbine efficiency.[23]

II. Negative Nonlinearity in BZT Working Fluids

The first requirement for a BZT–ORCE is to utilize a working fluid that exhibits BZT gasdynamic properties. BZT gasdynamic phenomena can be explained through the second law of thermodynamics in conjunction with elementary shock theory.[24] The relationship between the entropy change and specific volume across a weak shock is written as

$$\Delta s = -\left(\frac{\partial^2 p}{\partial \upsilon^2}\right)_s \frac{[\Delta \upsilon]^3}{12T} + \mathcal{O}([\Delta \upsilon]^4) \tag{1}$$

where $(\partial^2 p/\partial \upsilon^2)_s$ describes the concavity of an isentrope. For dilute gases far from the critical point, we have condition 1:

$$\left(\frac{\partial^2 p}{\partial \upsilon^2}\right)_s > 0$$

which requires $\Delta \upsilon < 0$ to satisfy the second law. For thermodynamic regions where the concavity of the isentropes is reversed, we have condition 2:

$$\left(\frac{\partial^2 p}{\partial \upsilon^2}\right)_s < 0$$

so that the specific volume $\Delta \upsilon$ must increase across the shock wave to have a corresponding increase in Δs. This indicates that expansion waves will steepen into shocks and compression waves will spread into fans, that is, the reverse behavior of flows having condition 1.

Using the van der Waals gas model, Bethe[24] and Zel'dovich[25] were the first to demonstrate thermodynamic regions that meet condition 2 for fluids with adequately large molecular weights and heat capacities. Thompson[26] was the first to recognize the importance of a fluid parameter Γ that governs the nonlinear dynamics of gases called the fundamental derivative of gasdynamics,

$$\Gamma = -\frac{\upsilon}{2}\left(\frac{\partial^2 p}{\partial \upsilon^2}\right)_s \Bigg/ \left(\frac{\partial p}{\partial \upsilon}\right)_s \tag{2}$$

written here in nondimensional form. In the most general sense, the sign and magnitude of Γ governs the rate of the distortion of wave characteristics. For fluids having condition 1, $\Gamma > 0$ because the denominator in Eq. (2), $(\partial p/\partial \upsilon)_s < 0$ everywhere, from the requirement of thermodynamic stability. The gasdynamics in the $\Gamma > 0$ region are said to exhibit positive nonlinearity. Flows with $\Gamma > 0$ everywhere behave classically, that is, compression waves steepen into shocks and expansion waves spread as fans. For a perfect gas with constant specific heats, the fundamental derivative reduces to $\Gamma = (\gamma + 1)/2$, which is always positive. Negative nonlinearity occurs in the thermodynamic region where $\Gamma < 0$ because the curvature of the isentropes is reversed, that is, condition 2. Flowfields for which Γ changes sign are said to have regions of mixed nonlinearity. An example of an isentrope inflection and the corresponding $\Gamma < 0$ region is evident in the p–υ diagram in Fig. 1. Thus, a fluid whose thermodynamic condition lies below the $\Gamma = 0$ line will behave nonclassically, that is, expansion waves steepen into expansion shocks and compression waves spread as fans. Drawing from the preceding discussion, a BZT fluid is specifically defined as a fluid that exhibits a $\Gamma < 0$ region above the coexistence curve in the vapor phase such as that shown in Fig. 1. In other words, the isentrope passing through the $\Gamma < 0$ region is inflected, indicative of the nonclassical fluid dynamic phenomena that occur in the negative nonlinear region.

Another important property of BZT gases is that shock strength is reduced up to an order of magnitude from that predicted in Eq. (1)

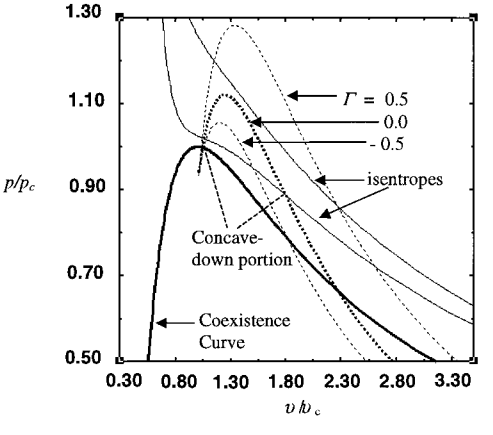

Fig. 1 Calculated from the van der Waals state equation, p–υ diagram for PP10 ($C_{13}F_{22}$) showing the coexistence curve, fundamental derivative Γ contours, and isentropes.

for thermodynamic conditions where $\Gamma \cong 0$. Reformulating Eq. (1) in terms of Γ, we have

$$\Delta s = -(a^2/6v^3T)\Gamma[\Delta v]^3 + \mathcal{O}([\Delta v]^4) \tag{3}$$

which shows that the fourth-order term becomes significant when the value of Γ is small.[27] Evident in Fig. 1, the value of Γ near the $\Gamma = 0$ contour on the low-density side remains small for small changes in volume. Thus, shock waves having jump conditions in the thermodynamic region near the low-density $\Gamma = 0$ contour are expected to be much weaker than normal.

The general strategy of a BZT–ORCE is to take advantage of the two dense gas properties described, that is, the spreading of compression waves where $\Gamma < 0$ and the weakening of compression shocks where $\Gamma \cong 0$. This requires a working fluid that exhibits a negative nonlinear region in the vapor phase. Whether a fluid is predicted to be BZT depends on the molecular weight and specific heat of the fluid in conjunction with the state equation used to describe the p–v–T behavior of the fluid. Using several gas models, Lambrakis and Thompson[28] and Thompson and Lambrakis[29] analytically show specific examples of existing hydrocarbons and fluorocarbons in which negative nonlinearity may be observed in the vapor phase region, for example, n-decane ($C_{10}H_{22}$) and perfluorodecalin ($C_{10}F_{18}$). Cramer[30] confirms these findings and extends the list of BZT fluids to several other commercially available fluorocarbons, for example, PP10 ($C_{13}F_{22}$) and FC-71 ($C_{18}F_{39}N$).

The size of the $\Gamma < 0$ region proportionally determines the effectiveness of a BZT working fluid. Here, the size of the negative nonlinear region refers to the total area enclosed within the coexistence curve and the $\Gamma = 0$ contour as shown in Fig. 1. Different state equations predict different nonlinearities for a given fluid. The $\Gamma < 0$ region for PP10 in Fig. 1 is calculated from the well-known van der Waals equation of state,

$$p = RT/(3v - b') - 3a/v^2 \tag{4}$$

where a and b' are the usual van der Waals constants. This is the simplest nonideal-gas state equation that can be used to model BZT gas effects. Derived from only two thermodynamic constraints on the critical isotherm, the van der Waals equation of state is quantitatively inaccurate near the vapor dome and is known to overpredict the size of the $\Gamma < 0$ region. The more accurate Martin–Hou state equation[31] predicts a much smaller $\Gamma < 0$ region for PP10 as shown in Fig. 2. In Fig. 2, the depiction of the Rankine cycle shows the basic strategy of operating the turbine stage in proximity to the negative nonlinear $\Gamma < 0$ region to reduce losses in the turbine. The formulation for the more sophisticated Martin–Hou state equation is written

$$p = \frac{RT}{v-b} + \frac{A_2 + B_2T + C_2e^{-kT/T_c}}{(v-b)^2} + \frac{A_3 + B_3T + C_3e^{-kT/T_c}}{(v-b)^3} + \frac{A_4}{(v-b)^4} + \frac{B_5T + C_5e^{-kT/T_c}}{(v-b)^5} \tag{5}$$

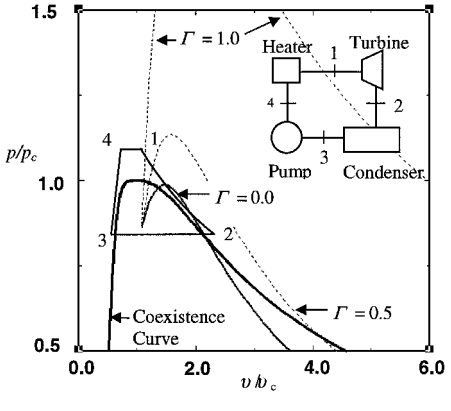

Fig. 2 Calculated from the Martin–Hou state equation, p–v diagram for PP10 ($C_{13}F_{22}$).

Derived from 10 thermodynamic constraints, the Martin–Hou state equation is designed specifically to model thermodynamic behavior in the high pressure–density region near the critical point. The only required parameters are the critical point values of the state variables and one point on the vapor pressure curve, making the Martin–Hou state equation very robust in terms of modeling various fluids. In Ref. 31, highly precise p–v–T data for CO_2 is used to assess the accuracy of the Martin–Hou state equation. For densities up to 1.3 times the critical density ρ_c, an average error of less than 0.2% is reported. From $1.3\rho_c$ to $1.4\rho_c$, the average error is around 1%. Large deviations from experimental data occur above $1.5\rho_c$. Similar results are also presented for several other gases.[32] This limiting value on the density is adequately large for the thermodynamic conditions of interest to this work.

At the present time, the Martin–Hou state equation[31] is arguably the best available gas model to manageably evaluate possible dense gas working fluids and to numerically model dense gas effects. The inaccuracy of the Martin–Hou gas model in predicting dense gas effects is likely to err on the conservative side. Cramer[30] points out that the negative-Γ region predicted by the Martin–Hou state equation[31] is unrealistically small. For perfluoromethyldecalin, both Lambrakis and Thompson[28] and Cramer[30] find that inflected downward curving isentropes [indicative of $\Gamma < 0$, see Eq. (2)] extend well into the $T > T_c$ region when the Martin–Hou equation[31] is used to interpolate manufacturer's data rather than computing Γ directly. The interpolation is thought to be a more accurate fit to the data, indicating that direct computation of the $\Gamma < 0$ region is conservative in size. Thus, the BZT effects on turbine performance from the computational analysis shown in this study are also likely to be conservative compared to the real effects.

III. BZT Gas Turbine Cascade Flow Strategy

The generation of compression shock waves in turbines is one of the major loss mechanisms encountered in Rankine cycle engines. Besides the adverse pressure gradient caused by the shock waves themselves, the collision of shocks with neighboring blades can result in boundary-layer separation causing further adverse pressure gradients as well as vibration and noise. Figure 3a shows a sketch of leading- and trailing-edge shock waves and boundary-layer separation that can create losses in supersonic turbine cascades. The disintegration of shocks in flowfield regions where $\Gamma < 0$ would prove very advantageous in reducing losses in turbine cascades. If $\Gamma < 0$ everywhere in the flow, the compression waves at the leading and trailing edges would take the form of fans instead of shocks as sketched in Fig. 3b, reducing the overall adverse pressure rise.

Boundary-layer separation arises mostly from the magnitude of the pressure gradient rather than the overall pressure rise, for example, see Ref. 33. Thus, the mild pressure gradients induced by the compression fans on neighboring blades would reduce the chances of boundary-layer separation. Cramer et al.[34] show such suppression of shock-induced boundary-layer separation for a dense gas flowfield with an oblique compression wave reflecting through a laminar boundary layer on a flat, adiabatic plate.

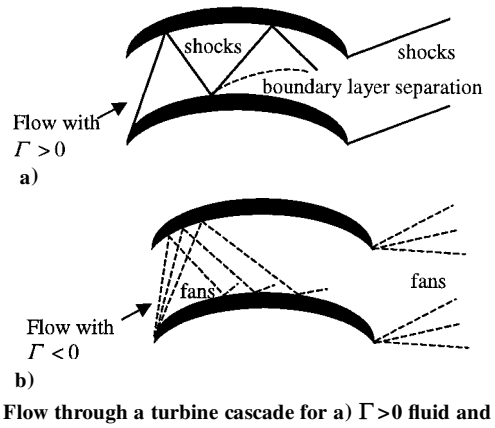

Fig. 3 Flow through a turbine cascade for a) $\Gamma > 0$ fluid and b) $\Gamma < 0$ (BZT) fluid.

Maintaining $\Gamma < 0$ throughout the entire turbine cascade flowfield such as is depicted in Fig. 3b is likely an ideal scenario. In reality, the flow through a turbine cascade consists of a complex wave field in which the flow encounters a series of compressions and expansions before reaching a nonuniform condition downstream of the cascade, for example, see Fig. 4. However, inflow conditions and blade designs that can retain the flow close to the negative Γ region as much as possible should still significantly reduce losses due to shock waves. Even in flow regions where $\Gamma > 0$, the strength and occurrences of shock discontinuities can be reduced if Γ remains small as is discussed in the preceding section.

The general strategy of operating the turbine stage in proximity to the $\Gamma < 0$ region is depicted in Fig. 2, which shows a preliminary sketch of how a supercritical Rankine cycle might be mapped onto the p–υ diagram of a dense gas working fluid. Heat is supplied in process 4–1 to the heater where the compressed liquid is converted to a superheated vapor at constant pressure. In process 1–2 the vapor is expanded adiabatically (isentropically in an ideal case) through a single-stage reaction turbine to produce a work output. For an impulse turbine stage, the flow is expanded through a stator stage or through nozzles. Shaft work is then generated as the flow is deflected through the impulse turbine, ideally without changing the thermodynamic condition of the gas. Vapor leaving the turbine enters the condenser where heat is removed until the vapor is condensed into the liquid state in process 2–3. Saturated liquid is then delivered to a pump, which raises the pressure of the liquid in process 3–4. The liquid is delivered back to the heater where the cycle then repeats. The inflow condition for a reaction turbine is generally located at point 1 whereas the inflow condition for an impulse turbine is generally located at point 2.

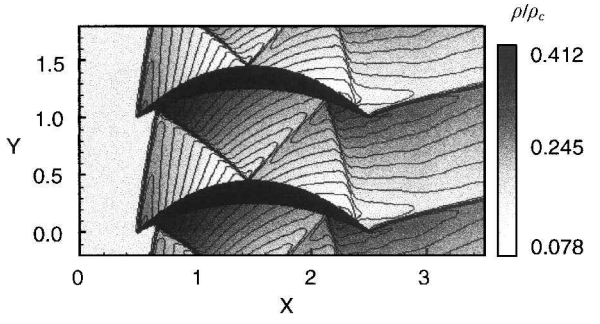

a) Toluene (C_7H_8), a conventional ORCE working fluid

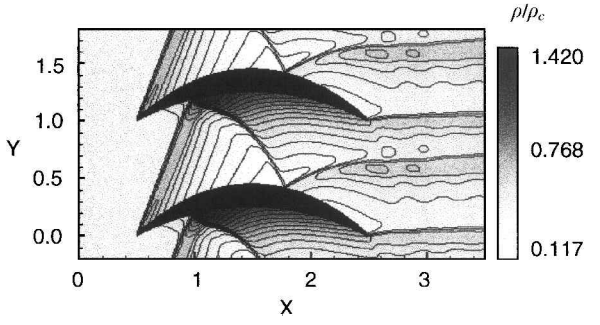

b) PP10 ($C_{13}F_{22}$), a BZT fluid at an inflow condition near the $\Gamma < 0$ region

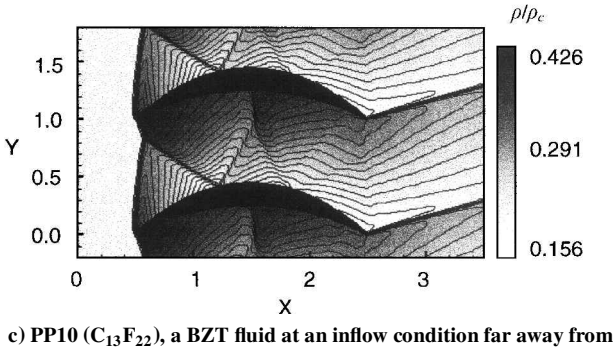

c) PP10 ($C_{13}F_{22}$), a BZT fluid at an inflow condition far away from the $\Gamma < 0$ region

Fig. 4 Impulse turbine cascade fields.

IV. Impulse Turbine Cascade Flows

Two-dimensional turbine cascade flowfields are investigated using the supersonic inviscid compressible flow solver (SCIFS).[23] SCIFS integrates the time-dependent Euler equations through a second-order time-space accurate flux-limited method developed by Davis.[35] The unique feature of SCIFS over many of the widely used compressible flow solver software packages is the incorporation of nonideal gas equations of state, including the Martin–Hou state equation.[31] SCIFS was successfully used to investigate both transient and steady two-dimensional dense gas flowfields. The SCIFS code has been validated through comparison with both experimental data[13] as well as analytical solutions of two-dimensional flowfields.[14,23] The well-resolved wave field structures computed through SCIFS closely agree with the experimental and analytical data. Thermodynamic conditions generally agree to within 1% of the data, including the jump conditions across shock waves. Solution convergence with mesh refinement is also verified for SCIFS.[13]

The specific geometry investigated is that of a symmetric impulse turbine cascade depicted in Fig. 5. Impulse cascades are designed to extract work from the fluid simply by turning the flow relative to the impulse blades without any pressure drop across the cascade, that is, zero reaction. As shown in the velocity vector diagram in Fig. 5, the turbine cascade moves in the y direction at velocity $\boldsymbol{V}_B$ relative to a stationary frame of reference. The incoming flow enters the cascade at velocity $\boldsymbol{V}_1$ at angle θ relative to the stationary frame and exits the cascade at velocity $\boldsymbol{V}_2$. Relative to the cascade, the flow enters at velocity $\boldsymbol{V}_{1R}$ at angle φ and exits with a velocity $\boldsymbol{V}_{2R}$ at angle β. All angles are measured relative to the y axis as indicated in Fig. 5 (Ref. 36).

An ideal flow through an impulse turbine cascade is isentropically turned through the blade passages such that the flow relative to the blades downstream of the cascade has thermodynamic conditions identical to the incoming flow. The only property change that occurs in the ideal flow is the reversal of the v (y-direction) component of velocity relative to the blades. Thus, for an ideal impulse cascade flow the magnitude of flow velocity relative to the blades does not change, that is, $\|\boldsymbol{V}_{2R}\| = \|\boldsymbol{V}_{1R}\|$, and the angle of the inflow relative to the cascade is equal to the angle of the outflow, that is, $\varphi = \beta$.

A simplified equation for the turbine hydraulic efficiency E_H, assuming zero reaction (no pressure drop) and fully ideal incoming nozzle flow is written[36]

$$E_H = 2(\boldsymbol{V}_B/\boldsymbol{V}_1)\left[\cos\theta - \boldsymbol{V}_B/\boldsymbol{V}_1 + \psi\cos\beta\sqrt{1 - 2(\boldsymbol{V}_B/\boldsymbol{V}_1)\cos\theta + \left(\boldsymbol{V}_B^2/\boldsymbol{V}_1^2\right)}\right] \tag{6}$$

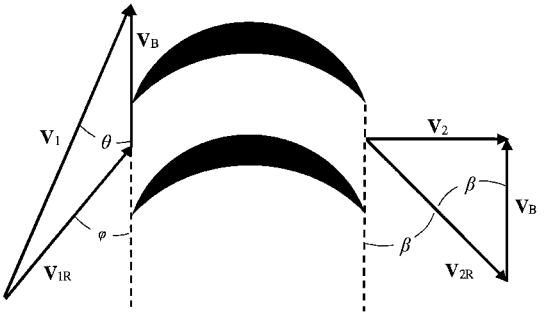

Fig. 5 Velocity vector diagram for a symmetric impulse turbine cascade.

The ratio V_B/V_1 is set equal to the ideal value of $V_B/V_1 = 0.5$ (see, for example, Ref. 37). The parameter ψ is the rotor velocity coefficient, which is the rotor exit velocity over the isentropic rotor exit velocity. In practice ψ is adjusted for several types of losses. For the purposes of this investigation, ψ is calculated as the ratio of the velocity magnitudes of the outflow and the inflow, that is, $\psi = V_{R2}/V_{R1}$. Thus, for the ideal impulse turbine $\psi = 1$. Losses due to shock waves would decrease the velocity magnitude such that $\psi < 1$. Note that E_H is also a function of the angle of the exit flow relative to the cascade, that is, β. Losses due to shock waves will inhibit the full turning of the flow such that $\beta \neq \varphi$, as is the case for an ideal impulse turbine. Note that the hydraulic efficiency E_H is not the same as the adiabatic efficiency, a more commonly known thermodynamic parameter that is generally defined as the ratio of the actual work over the isentropic (reversible) work.[36] The hydraulic efficiency is, however, a performance parameter that is commonly used by ORCE manufacturers and is used here for that reason.

The flowfields for the cascades shown in Fig. 4 have an incoming Mach number of $M_1 = 1.5$ for a symmetric impulse turbine blade geometry that is designed to turn the flow a total of 50 deg. The inlet Mach number is held constant at $M_1 = 1.5$ for all of the flowfields investigated because the Mach number is usually one of the primary design parameters for an ORCE turbine.[37] The upper and lower surfaces of the blades are circular arcs with chord $c = 2.0$ relative to the spatial coordinates of the computational domain and maximum thickness of $t/c = 0.095$. The blades are separated by a distance of $d/c = 0.5$. For this particular geometry $\theta = 38$ deg and $\beta = 65$ deg for an ideal impulse turbine. Thus, the maximum hydraulic efficiency for the simulated impulse turbine cascade is calculated from Eq. (6) to be $E_{H\text{-max}} = 0.823$.

One performance parameter chosen to evaluate the quality of the flow through the cascade is the pressure ratio p_2/p_1. The subscripts 1 and 2 refer to the inflow condition and outflow condition, respectively. The pressure is chosen as a thermodynamic performance parameter because pressure is typically a primary design parameter for ORCEs (e.g., see Ref. 4) and the pressure ratio is directly indicative of shock strength (e.g., through the well-known Rankine–Hugoniot relations[36]) and subsequently shock-related losses. The rotor velocity coefficient ψ and the ratio of efficiency over the maximum efficiency (i.e., $E_H/E_{H\text{-max}}$) are also chosen as performance parameters.

Table 1 lists the specified fluids and inflow conditions for a conventional ORCE working fluid and inflow condition (case 4A), a BZT working fluid with an inflow condition in proximity to the $\Gamma < 0$ region (case 4B), and the same BZT working fluid with an inflow condition relatively far from the negative nonlinear region (case 4C). The performance parameters just discussed are also tabulated for each case where properties downstream of the cascade are obtained from the average values at the outflow boundary.

The values of the performance parameters do not provide a completely realistic analysis of turbine efficiency because the only losses investigated for the inviscid flow are those due to shock waves. Boundary-layer separation would cause further degradation in the flow. Whereas losses due to boundary-layer separation cannot be directly investigated here, reductions in the strength of waves reflecting from the blade surfaces are expected to contribute to the suppression of boundary-layer separation. As mentioned earlier, Cramer et al.[34] show such suppression of shock-induced boundary-layer separation for a dense gas flowfield with an oblique compression wave reflecting through a laminar boundary layer on a flat, adiabatic plate.

Of course, there are other realistic losses not accounted for as well, such as frictional losses, thermal losses, and leakage around the tip of the blade. Collectively, these losses result in an efficiency that is typically in the range of $0.6 < E_H < 0.8$ for conventional impulse turbines.[37] The idea of the work presented here is to demonstrate favorable trends of improved flow through the cascade due to the properties of BZT fluids. The performance parameters in Table 1 provide a good rule of thumb in recognizing such trends, that is, the closer the parameters are to unity, the higher the quality of flow through the cascade.

All cases use the Martin–Hou[31] gas model to compare a cascade flow with toluene (C_7H_8), a fluid commonly used in many ORCEs, to a cascade flow with PP10, a heavy fluorocarbon that is classified as a BZT fluid, indicated by the negative-Γ region in Fig. 2. Inflow conditions for the toluene flow of case 4A in Table 1 are approximated using a p–h diagram from a manufacturer's report for a 20-kW solar powered ORCE.[38] Toluene is not BZT because it is not heavy enough to exhibit a $\Gamma < 0$ region. The wave field for case 4A is displayed in Fig. 4a. The shock wave originating from the leading edge of the upper surface of the blade reflects twice on the upper surface and twice on the lower surface as seen in the isopycnics displayed in Fig. 4a. The multiple reflections create ample opportunity for boundary-layer separation. A strong shock wave at the trailing edge increases the pressure further. The average outflow Mach number decreases from the inflow value from $M_1 = 1.50$ to $M_2 = 1.31$. The pressure ratio $p_2/p_1 = 1.32$ indicates the drag losses due to the shock waves. A rotor velocity coefficient value of $\psi = 0.811$ decreases the efficiency to 75.2% of the maximum efficiency (i.e., $E_H/E_{H\text{-max}} = 0.752$) due to the shock wave losses alone.

Figure 4b illustrates the wave field of case 4B for PP10. Inflow thermodynamic conditions are chosen to the right of the $\Gamma < 0$ region located at position 2 of the Rankine cycle diagram in Fig. 2. The resulting wave field is significantly different from that of the conventional working fluid of case 4A. The shock emanating from the leading edge of the upper surface terminates at a triple point with a short Mach stem originating from the lower surface. Just downstream of the leading-edge shock, isopycnics indicate an expansion fan that initially converges above the blade rather than spreading, as is usually the case for dilute, nondense gas flows. The reflected shock wave originating from the triple point reflects from the upper surface of the blade, then weakens and appears to spread downstream of the cascade. The single occurrence of shocks on the upper and lower surfaces is likely to reduce losses due to boundary-layer separation over the multiple reflection of the shock such as that of case 4A. A detailed analysis of the trailing edge wave in Fig. 4b determines the wave to be a slowly spreading compression fan in contrast to the strong trailing-edge shock wave in Fig. 4a.

Evident in Table 1, the performance parameters of case 4B for PP10 are much improved over case 4A for toluene. The average outflow Mach number increases from the inflow value to $M_2 = 1.62$. The pressure ratio $p_2/p_1 = 1.09$ is significantly lower than that corresponding to the toluene flow of case 4A. An increased velocity rotor coefficient $\psi = 0.895$ results in an improved efficiency ratio of $E_H/E_{H\text{-max}} = 0.781$.

Table 1 ORCE working fluids listing critical point values, inflow conditions, and performance parameters[a]

Case	Fluid	Formula	p_c, atm	T_c, K	ρ_1	p_1	Γ_1	p_2/p_1	ψ	$E_H/E_{H\text{-max}}$
4A	Toluene	C_7H_8	40.4	591.8	0.154	0.420	0.80	1.32	0.811	0.752
4B	PP10	$C_{13}F_{22}$	16.0	632.2	0.391	0.806	0.24	1.09	0.895	0.781
4C	PP10	$C_{13}F_{22}$	16.0	632.2	0.200	1.200	1.00	1.19	0.894	0.736

[a]Parameters for a 25-deg symmetrical impulse turbine cascade with $M_1 = 1.5$. Inflow variables are normalized to the critical point values. PP10, the BZT working fluid, shows improved performance parameters over toluene, the conventional ORCE working fluid.

Note that simply utilizing a BZT working fluid that exhibits a $\Gamma < 0$ region is not sufficient to maximize the reduction in losses due to shock waves. Operating near the $\Gamma < 0$ region is also necessary. This is demonstrated in case 4C. The fluid (PP10), cascade geometry, and inflow Mach number $M_1 = 1.5$ are identical to case 4B. The inflow condition, however, is located far away from the $\Gamma < 0$ region at $p/p_c = 1.2$ and $\rho/\rho_c = 0.2$. Shown in Fig. 4c, the BZT effects that are observed in Fig. 4b are no longer evident. Rather, the appearance of the wave field more closely resembles that of the conventional fluid in Fig. 4a with multiple shock reflections and a strong trailing-edge shock wave. The average Mach number at the outflow is reduced from the inflow value to $M_2 = 1.34$. This is in contrast to the increase in Mach number across the cascade observed in case 4B.

The absence of negative nonlinear effects on the performance parameters for case 4C is also evident. The pressure ratio $p_2/p_1 = 1.19$ of case 4C is higher than that of case 4B, whereas the efficiency ratio is the lowest of all three cases at $E_H/E_{H\text{-max}} = 0.736$.

V. Conclusions

The purpose of the work presented here is to introduce BZT gasdynamics in the context of ORCE technology and to demonstrate the proof-of-concept application of a BZT working fluid to improve flow through an ORCE turbine. To take advantage of BZT gasdynamic properties, the ORCE working fluid must exhibit a region of negative nonlinearity ($\Gamma < 0$) in the vapor phase. The strategy of operating the turbine stage in proximity to the $\Gamma < 0$ region is shown to be feasible for a Rankine cycle.

Improved cascade flow is found for PP10, a proposed BZT fluid, over that of toluene, a conventional ORCE working fluid. All performance parameters for the PP10 cascade flow are enhanced compared to that of the toluene flow due to negative nonlinear effects exhibited by PP10. The 3% improvement in efficiency demonstrated by these results would be significant enough to be considered a major breakthrough in ORCE technology (private communication with W. Batton, Vice-President of Barber–Nichols, Inc. in 1997). This predicted improvement in efficiency is likely to be conservative for the following reasons:

1) The Martin–Hou state equation used in the SCIFS computations is likely to be conservative in the predicted size of the $\Gamma < 0$ region for PP10 according to the studies of Lambrakis and Thompson[28] and Cramer[30] (see Sec. II for a detailed discussion). Thus, the dense gas effects in a prototype engine are likely to be enhanced due to a larger negative nonlinear region.

2) The working fluid chosen for this study, PP10, is predicted to exhibit a relatively small $\Gamma < 0$ region. Other fluids exist (e.g., PP25) that are predicted to have larger negative nonlinear regions that would enhance dense gas effects and further improve efficiency.

3) The efficiency improvements from the results presented here are due solely to a reduction in the wave drag created by the shock waves. The decreased reflections and strengths of shock waves due to the dense gas effects are also expected to reduce turbine losses due to flow separation, resulting in a higher net gain in efficiency than that predicted here.

4) The configuration of the inflow condition and blade profile used for this study is only one of a large number of possible configurations and is not likely the optimal configuration to maximize the efficiency improvement.

Note that simply utilizing a BZT working fluid that exhibits a $\Gamma < 0$ region is not sufficient to maximize the reduction in losses due to shock waves. Operating the turbine cascade at a pressure and temperature near the $\Gamma < 0$ region is also necessary.

The critical values of conventional fluids such as toluene and the dense gas fluids such as PP10 are similar. Thus, standard ORCE design and fabrication methods can be used to design and build BZT–ORCEs. Using a BZT working fluid would not require any radical change in ORCE fabrication and operation.

Future work will involve detailed investigation of specific candidate BZT working fluids as well as parametric analyses for various inflow conditions and turbine cascade geometries.

References

[1]Curran, H. M., "Use of Organic Working Fluids in Rankine Engines," *Journal of Energy*, Vol. 5, No. 4, 1981, pp. 218–223.

[2]Monahan, J., and McKenna, R., "Development of a 1-kW Organic Rankine Cycle Power Plant for Remote Applications," *Proceedings of the 11th Intersociety Energy Conversion Engineering Conference*, Paper 769199, Aug. 1976.

[3]Barber, R. E., "Solar-Powered Organic Rankine Cycle Engines—Characteristics and Costs," *Proceedings of the 11th Intersociety Energy Conversion Engineering Conference*, Paper 769200, Aug. 1976.

[4]Batton, W., and Barber, R. E., "Rankine Engine Solar Power Generation, Part II—The Power Generation Module," American Society of Mechanical Engineers, Paper 81-WA/Sol-23, Nov. 1981.

[5]Prigmore, D. R., and Nichols, K. E., "Recent Developments in the Organic Rankine Cycle Heat Engine Field," *Proceedings of the 15th Intersociety Energy Conversion Engineering Conference*, AIAA, Washington, DC, Aug. 1980.

[6]Barber, R. E., "Solar and Geothermal Rankine Cycle Engines Can Convert Petroleum Industry Waste Heat into Electrical Power," American Society of Mechanical Engineers, Paper 80-Pet-27, Nov. 1979.

[7]Cheek, R. M., and Lacey, P. D., "600 kW Organic Rankine Cycle Waste Heat Power Conversion System," *Proceedings of the 12th Intersociety Energy Conversion Engineering Conference*, American Nuclear Society, Washington, DC, Aug. 1977, pp. 1095–1099.

[8]Cramer, M. S., "Nonclassical Dynamics of Classical Gases," *Nonlinear Waves in Real Fluids*, Springer–Verlag, Berlin, 1991, pp. 91–145.

[9]Schnerr, G. H., and Leidner, P., "Diabatic Supersonic Flows of Dense Gases," *Physics of Fluids*, Vol. 3, No. 10, 1991, pp. 2445–2458.

[10]Cramer, M. S., Kluwick, A., Watson, L. T., and Pelz, W., "Dissipative Waves in Fluids Having Both Positive and Negative Nonlinearity," *Journal of Fluid Mechanics*, Vol. 169, 1986, pp. 323–336.

[11]Thompson, P. A., Carofano, G. C., and Kim, Y., "Shock Waves and Phase Changes in a Large-Heat-Capacity Fluid Emerging from a Tube," *Journal of Fluid Mechanics*, Vol. 166, 1986, pp. 57–92.

[12]Argrow, B. M., "Computational Analysis of Dense Gas Shock Tube Flow," *Shock Waves*, Vol. 6, No. 4, 1996, pp. 241–248.

[13]Brown, B. P., and Argrow, B. M., "Two-Dimensional Shock Tube Flow for Dense Gases," *Journal of Fluid Mechanics*, Vol. 349, 1997, pp. 95–115.

[14]Brown, B. P., and Argrow, B. M., "Nonclassical Dense Gas Flows for Simple Geometries," *AIAA Journal*, Vol. 36, No. 10, 1998, pp. 1842–1847.

[15]Aldo, A. C., and Argrow, B. M., "Dense Gas Flow in Minimum Length Nozzles," *Journal of Fluids Engineering*, Vol. 117, No. 2, 1994, pp. 270–276.

[16]Anders, J. B., "Heavy Gas Wind-Tunnel Research at Langley Research Center," American Society of Mechanical Engineers, Paper 93-Fe-5, Feb. 1993.

[17]Kluwick, A., "Transonic Nozzle Flow of Dense Gases," *Journal of Fluid Mechanics*, Vol. 217, 1993, pp. 661–688.

[18]Schnerr, G. H., and Leidner, P., "Two-Dimensional Nozzle Flow of Dense Gases," American Society of Mechanical Engineers, Paper 93-Fe-8, June 1993.

[19]Anderson, W. K., "Numerical Study Using Sulfur Hexafluoride as a Wind-Tunnel Test Gas," *AIAA Journal*, Vol. 29, No. 12, 1991, pp. 2179, 2180.

[20]Schnerr, G. H., and Leidner, P., "Numerical Investigation of Axial Cascades for Dense Gases," *Proceedings of the Pacific International Conference on Aerospace Science and Technology*, Taiwan, ROC, Dec. 1993.

[21]Monaco, J. F., Cramer, M. S., and Watson, L. T., "Supersonic Flows of Dense Gases in Cascade Configurations," *Journal of Fluid Mechanics*, Vol. 330, 1997, pp. 31–59.

[22]Maizza, V., "The Use of Unconventional Fluids for Single Stage Supersonic Turbines of Low Power Output," *Proceedings of the 11th Intersociety Energy Conversion Engineering Conference*, Paper 769203, Aug. 1976.

[23]Brown, B. P., "Two-Dimensional Dense Gas Dynamics," Ph.D. Dissertation, Dept. of Aerospace Engineering Sciences, Univ. of Colorado, Boulder, CO, July 1997.

[24]Bethe, H. A., "The Theory of Shock Waves for an Arbitrary Equation of State," Office of Scientific Research and Development, Report No. 545, Washington, DC, 1942.

[25]Zel'dovich, Ya. B., "On the Possibility of Rarefaction Shock Waves," *Zhurnal Eksperimentalnoi i Teoreticheskoi Fiziki*, Vol. 4, 1946, pp. 363, 364 (in Russian).

[26]Thompson, P. A., "A Fundamental Derivative in Gas Dynamics," *Physics of Fluids*, Vol. 14, No. 9, 1971, p. 1843.

[27]Cramer, M. S., and Kluwick, A., "On the Propagation of Waves Exhibiting Both Positive and Negative Nonlinearity," *Journal of Fluid Mechanics*, Vol. 142, No. 9, 1984, pp. 9–37.

[28]Lambrakis, K. C., and Thompson, P. A., "Existence of Real Fluids with a Negative Fundamental Derivative Γ," *Physics of Fluids*, Vol. 15, No. 5, 1972, pp. 933–935.

[29]Thompson, P. A., and Lambrakis, K. C., "Negative Shock Waves," *Journal of Fluid Mechanics*, Vol. 60, Pt. 1, 1973, pp. 187–208.

[30]Cramer, M. S., "Negative Nonlinearity in Selected Fluorocarbons," *Physics of Fluids*, Vol. 1, No. 11, 1989, pp. 1894–1897.

[31]Martin, J. J., and Hou, Y. C., "An Improved Equation of State for Gases," *AIChE Journal*, Vol. 5, No. 2, 1959, pp. 142–151.

[32]Martin, J. J., and Hou, Y. C., 1955, "Development of an Equation of State for Gases," *AIChE Journal*, Vol. 1, No. 2, 1955, pp. 142–151.

[33]Schlichting, H., *Boundary Layer Theory*, McGraw–Hill, New York, 1968, pp. 33–35.

[34]Cramer, M. S., Park, S., and Watson, L. T., "Suppression of Shock-Induced Separation in Dense Gases," *Proceedings of the 20th International Symposium on Shock Waves*, World Scientific, Singapore, Republic of Singapore, 1997, pp. 783–788.

[35]Davis, S. F., "A Simplified TVD Finite Difference Scheme via Artificial Viscosity," *SIAM Journal on Scientific and Statistical Computing*, Vol. 8, No. 1, 1987, pp. 1–18.

[36]van Wylen, G. J., Sonntag, R. E., and Borgnakke, C., *Fundamentals of Classical Thermodynamics*, Wiley, New York, 1994, pp. 691–701.

[37]Nichols, K. E., "How to Select Turbomachinery for Your Application," Barber Nichols Engineering Co., Internal Rept., Arvada, CO, 1982.

[38]Barber, R. E., and Boda, F. P., "Organic Rankine Power Conversion Subsystem Development for the Small Community Solar Thermal Power System," Dept. of Energy Solar Thermal Power and Annual Program Review, Washington, DC, 1970.